Theory of director precession and nonlinear waves in nematic liquid crystals under elliptical shear

A. P. Krekhov and L. Kramer*
Physikalisches Institut, Universität Bayreuth, D-95440 Bayreuth, Germany
(Received 15 March 2005; published 15 September 2005)

We study theoretically the slow director precession and nonlinear waves observed in homeotropically oriented nematic liquid crystals subjected to circular or elliptical Couette and Poiseuille flow and an electric field. From a linear analysis of the nematodynamic equations it is found that in the presence of the flow the electric bend Fréedericksz transition is transformed into a Hopf-type bifurcation. In the framework of an approximate weakly nonlinear analysis we have calculated the coefficients of the modified complex Ginzburg-Landau equation, which slightly above onset describes nonlinear waves with strong nonlinear dispersion. We also derive the equation describing the precession and waves well above the Fréedericksz transition and for small flow amplitudes. Then the nonlinear waves are of diffusive nature. The results are compared with full numerical simulations and with experimental data.

DOI: 10.1103/PhysRevE.72.031705 PACS number(s): 61.30.Gd, 64.70.Md, 47.20.Ky

I. INTRODUCTION

A nematic liquid crystal is characterized by long-range orientational order of the molecules along an axis $\boldsymbol{n}$, the director, which may vary slowly in space and time. A particularly interesting configuration is obtained when $\boldsymbol{n}$ is aligned homeotropically—i.e., perpendicularly—at the bounding plates of a nematic layer and distorted inside by an external field, not destroying the rotational invariance around the symmetry axis of the system. There are two established methods to achieve this goal. First, by using a material with negative dielectric anisotropy and applying a sufficiently strong electric field across the layer, a bend Fréedericksz transition (FT) will occur, which generates such a configuration [1]. Second, one may use a strong, circularly polarized laser beam at normal incidence to produce an optical FT [2].

Clearly in such a situation the director configuration resulting from the FT spontaneously breaks rotational invariance. In fact, rotating the whole configuration around the axis perpendicular to the plane of the nematic layer by some angle corresponds to a symmetry operation of the system. Thus there exists a neutral (Goldstone) mode. As a consequence, breaking helicity—i.e., reflection symmetry in the plane of the layer—will in general lead to a precession of the director. In the optical case helicity is in fact broken from the beginning on and the director precession is a well-known effect leading to more complex dynamic phenomena at larger intensities [3,4]. In the applied electric field case one needs additional effects like imposing a circular shear flow on the nematic layer.

During the last two decades shear flow experiments have indeed been carried out and the slow precession generated by circular and elliptical shear in the Fréedericksz-distorted state has been observed recently [5]. Well above the FT the precession was accompanied by nonlinear diffusive waves. Slightly above the FT spatiotemporally chaotic dynamics was observed, and at somewhat higher fields nonlinear dispersive waves forming rotating spirals appeared. Neglecting elasticities and neglecting the influence of the director distortion on the flow field an exact solution of the director dynamic equations was found that captures the precession and predicts a reversal for non-flow-aligning materials [5,6]. This analysis is expected to be valid for high frequencies and not too near to the FT. Thus, it was not possible to describe the dependence of the precession frequency on the applied electric field, especially close to the FT, and, of course, not the wave phenomena, which are generated by the elastic coupling.

In this work we extend the theory of the precession phenomena to include (i) the elastic coupling of the director, (ii) the feedback on the velocity field (back flow), and (iii) slow modulations in the plane of the layer in order to capture the wave phenomena. It turns out that the inclusion of back flow is decisive to understand the behavior near the FT. In Sec. II we present the general formulation of the problem and explain the numerical procedure used for direct simulations. In Sec. III we give a linear and weakly nonlinear analysis of the FT in the presence of circular shear flow. It demonstrates that the FT is transformed by the presence of the flow into a Hopf bifurcation and shows that nonlinear dispersion is strong, so spatiotemporally chaotic dynamics and dispersive waves are to be expected. In Sec. IV a phase-wave analysis valid well above the FT is presented for the general elliptic case. It demonstrates that in this range one will have diffusive phase waves in the system. Finally, in Sec. V the results are discussed and put into perspective.

Director precession and phase waves have been observed previously in cells that were excited piezoelectrically at frequencies around 50 kHz [7,8]. The piezocrystal formed one of the bounding plates. Phenomena reminiscent of the phase waves were also seen in planar and homeotropic cells without electric field at frequencies $10\ \text{kHz} < f < 1\ \text{MHz}$ [9]. There the waves originated from orientational defects at the surface. Although in these cases the precise form of the excitation was not clear, it appears likely that the mechanisms

*Deceased.

discussed here form the basis of the phenomena.

II. THEORETICAL BACKGROUND

We consider a nematic layer of thickness d confined between two infinite parallel plates. Oscillatory elliptical Couette flow can be imposed by one plate oscillating periodically in the form

$$x(t) = A_x \sin(\omega t), \quad y(t) = A_y \sin(\omega t + \phi) \tag{1}$$

or by applying the two rectilinear components to the two plates. Oscillatory Poiseuille flow is generated by an alternating pressure gradient applied in the plane of the layer ($0 \leqslant x \leqslant L_x$, $0 \leqslant y \leqslant L_y$):

$$\frac{\partial p}{\partial x} = \frac{\Delta P_x}{L_x} \cos(\omega t), \quad \frac{\partial p}{\partial y} = \frac{\Delta P_y}{L_y} \cos(\omega t + \phi), \tag{2}$$

with the pressure drops ΔP_x, ΔP_y over the lengths L_x, L_y, respectively. The phase shift ϕ between the velocity oscillations in the x and y directions could in particular be $\pm\pi/2$ which correspond to clockwise-counterclockwise velocity rotation. The director $\boldsymbol{n}$ at the boundaries is oriented homeotropically (along the z axis), and the electric field $\boldsymbol{E}$ is applied along the z direction. The case of a nematic with negative dielectric anisotropy is considered.

Note that in the absence of an electric field for Couette flow (1) above some critical shear amplitudes one has a direct transition to convective patterns with the orientation of the roll axis depending on the ellipticity of the shear (ratio A_x/A_y) [10]. A detailed theoretical analysis of this kind of instability shows that the driving mechanism results from the steady forces generated by the nonlinear terms in the viscous stress tensor and the critical shear amplitude is [11,12]

$$\frac{A_x A_y}{d^2} \simeq \frac{2K\pi^2}{\eta d^2 \omega}, \tag{3}$$

where K is an elastic constant and η an effective viscosity of the nematic. In the following we will focus on flow amplitudes much smaller than the ones given in Eq. (3).

The standard set of nematodynamic equations [13] consists of the director equation

$$\gamma_1(\partial_t + \boldsymbol{v}\cdot\boldsymbol{\nabla})\boldsymbol{n} = \gamma_1 \boldsymbol{\Omega}\times\boldsymbol{n} + \underline{\underline{\delta}}^{\perp}(-\gamma_2 \underline{\underline{A}}\boldsymbol{n} + \boldsymbol{h}^r), \tag{4}$$

where γ_1, γ_2 are rotational viscosities:

$$\gamma_1 = \alpha_3 - \alpha_2, \quad \gamma_2 = \alpha_6 - \alpha_5 = \alpha_3 + \alpha_2. \tag{5}$$

Here α_k denote the Leslie viscosity coefficients and we have used the Parodi relation. In Eq. (4) $\boldsymbol{\Omega} = (\boldsymbol{\nabla}\times\boldsymbol{v})/2$ is the local fluid rotation, $\delta_{ij}^{\perp} = \delta_{ij} - n_i n_j$ is the projection tensor which imposes the normalization of $\boldsymbol{n}$ ($\boldsymbol{n}^2 = 1$), $A_{ij} = (v_{i,j} + v_{j,i})/2$ is the hydrodynamic strain, and $\boldsymbol{h}^r$ is the force on the director derived from the orientational free energy density:

$$h_i^r = \frac{\partial}{\partial x_j}\frac{\partial F}{\partial n_{i,j}} - \frac{\partial F}{\partial n_i} \tag{6}$$

($,j$ denotes the partial derivative with respect to the spatial coordinate x_j), where F is

$$F = \frac{1}{2}\{K_{11}(\boldsymbol{\nabla}\cdot\boldsymbol{n})^2 + K_{22}[\boldsymbol{n}\cdot(\boldsymbol{\nabla}\times\boldsymbol{n})]^2 + K_{33}[\boldsymbol{n}\times(\boldsymbol{\nabla}\times\boldsymbol{n})]^2 - \epsilon_0\epsilon_a(\boldsymbol{E}\cdot\boldsymbol{n})^2\}, \tag{7}$$

with the elastic constants K_{11}, K_{22}, and K_{33} for "splay," "twist," and "bend" deformations, respectively.

The Navier-Stokes equation (momentum balance) has the form

$$\rho\frac{d}{dt}v_i = -p_{,i} + T_{ji,j}, \tag{8}$$

where ρ is the mass density, p is the pressure, and the stress tensor T_{ij} has elastic and viscous parts

$$T_{ij} = s_{ij} + t_{ij},$$

$$s_{ij} = -\frac{\partial F}{\partial n_{k,i}} n_{k,j},$$

$$t_{ij} = \alpha_1 n_k n_m A_{km} n_i n_j + \alpha_2 n_i N_j + \alpha_3 n_j N_i + \alpha_4 A_{ij} + \alpha_5 n_i n_k A_{kj} + \alpha_6 n_j n_k A_{ki}, \tag{9}$$

where $\boldsymbol{N} = (\partial_t + \boldsymbol{v}\cdot\boldsymbol{\nabla})\boldsymbol{n} - \boldsymbol{\Omega}\times\boldsymbol{n}$. In addition we have the incompressibility condition $\boldsymbol{\nabla}\cdot\boldsymbol{v} = 0$.

We first focus on the homogeneous (in the plane of the layer) precession of the director. Thus we assume

$$\boldsymbol{n} = \{n_x(z,t), n_y(z,t), n_z(z,t)\},$$

$$\boldsymbol{v} = \{v_x(z,t), v_y(z,t), 0\}. \tag{10}$$

Clearly the incompressibility condition is satisfied automatically.

It is useful to introduce the dimensionless variables

$$\tilde{z} = z/d, \quad \tilde{t} = \omega t, \quad \tilde{\mathbf{v}} = \mathbf{v}/(d\omega), \quad e^2 = E^2/E_F^2,$$

$$E_F = \frac{\pi}{d}\sqrt{\frac{K_{33}}{\epsilon_0|\epsilon_a|}}, \quad k_i = K_{ii}/K_{33}, \quad \tilde{\alpha}_i = \alpha_i/\gamma_1,$$

$$\epsilon = \frac{1}{\tau_d\omega}, \quad \tau_d = \frac{\gamma_1 d^2}{K_{33}}, \quad \delta = \frac{d^2}{l^2}, \quad l = \sqrt{\frac{\gamma_1}{\rho\omega}}. \tag{11}$$

Moreover, we reformulate the nematodynamic equations in terms of the complex fields

$$N = n_x + i n_y, \quad V = v_x + i v_y. \tag{12}$$

This leads to (we omit tildes on the variables, but keep it for clarity on the viscosities)

$$N_{,t} - \epsilon\left\{\pi^2 e^2(1-|N|^2)N - k_1 n_z n_{z,zz} N + k_3\left[N_{,zz} - \frac{1}{2}N(N\bar{N}_{,zz} + \bar{N}N_{,zz})\right] - (k_3 - k_2)\left[\frac{1}{2}N(B^2 + iB_{,z}) + iN_{,z}B\right]\right\} + \tilde{\alpha}_2 n_z V_{,z} - \frac{1}{2}(\tilde{\alpha}_2 + \tilde{\alpha}_3) n_z N(N\bar{V}_{,z} + \bar{N}V_{,z}) = 0, \tag{13}$$

with $n_z = \sqrt{1-|N|^2}$, $B = i(N\bar{N}_{,z} - \bar{N}N_{,z})$, and

$$\delta V_{,t} + p_{0,\eta} - \partial_z \Bigg\{ \tilde{\alpha}_2 n_z N_{,t} + \tilde{\alpha}_3 n_{z,t} N + \frac{1}{2}[\tilde{\alpha}_4 + (-\tilde{\alpha}_2 + \tilde{\alpha}_5) \times (1 - |N|^2)] V_{,z} + \frac{1}{2}\left[\frac{1}{2}(\tilde{\alpha}_3 + \tilde{\alpha}_6) + \tilde{\alpha}_1(1 - |N|^2)\right] \times N(N\bar{V}_{,z} + \bar{N}V_{,z}) \Bigg\} = 0, \tag{14}$$

where $\eta = x - iy$, $\partial_\eta = \partial_x + i\partial_y$, and $\bar{N}$, $\bar{V}$ stand for the complex conjugate. The boundary conditions in case of strong homeotropic anchoring, which we will consider throughout this work, are

$$N(z = \pm 1/2) = 0. \tag{15}$$

For the complex velocity V one has, for Couette flow,

$$p_0 = 0,$$

$$V(z = +1/2) = a[\cos(t) + ib\cos(t - \pi/2)],$$

$$V(z = -1/2) = 0, \tag{16}$$

with $a = A_x/d$ and $ab = A_y/d$ where $0 \leqslant b \leqslant 1$ characterizes the ellipticity of the flow. In the case of Poiseuille flow,

$$p_{0,\eta} = a[\cos(t) + ib\cos(t - \pi/2)],$$

$$V(z = \pm 1/2) = 0, \tag{17}$$

and $a = (\Delta P_x/L_x)[d/(\gamma_1\omega)]$ and $ab = (\Delta P_y/L_y)[d/(\gamma_1\omega)]$. For definiteness we choose the phase shift equal to $-\pi/2$ between the velocity oscillations in x and y directions which correspond to a counterclockwise rotation.

Direct numerical simulations of Eqs. (13) and (14) for Couette and Poiseuille flow were performed for material parameters corresponding to the substances Phase 5A (Merck) and MBBA (see the Appendix for the material parameters). We used central finite differences for the spatial derivatives and the predictor-corrector scheme for the time discretization. For both types of flow and an electric field E below the bend Fréedericksz transition E_F the director rotates with the flow frequency ω. It corotates with the elliptic shear on a cone with the cone axis along z. Thus the projection of the director onto the x-y plane averaged over one flow period is zero. In contrast, for an electric field E above some critical value E_c in addition to the rotation the director performs a slow precession. The projection of the director averaged over the flow period is nonzero and slowly rotates. The simulations show that the transition to slow precession is through a Hopf-type bifurcation and the critical electric field E_c actually slightly above the zero-flow value E_F. At E_c the precession amplitude increases continously without hysteresis.

For both types of flow the precession frequency Ω is very small. For flow amplitudes that are about the same in the x and y directions and for given E and ω we find $\Omega \sim a_x a_y$, where $a_x = A_x/d$, $a_y = A_y/d$ for Couette flow and $a_x = (\Delta P_x/L_x)[d/(\gamma_1\omega)]$ and $a_y = (\Delta P_y/L_y)[d/(\gamma_1\omega)]$ for Poiseuille flow are the dimensionless flow displacement amplitudes. The precession frequency also depends on the electric field E and on the flow frequency ω (see Figs. 1 and 2).

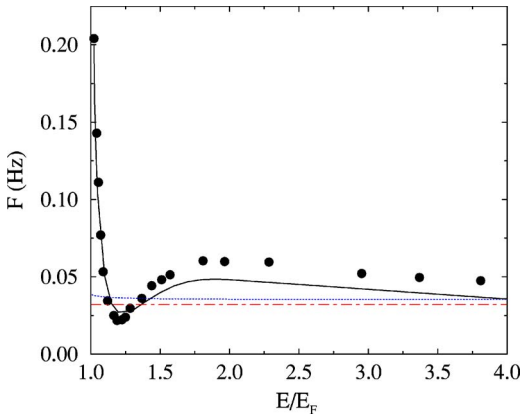

FIG. 1. (Color online) Precession frequency $F = \Omega/2\pi$ as a function of electric field E/E_F for circular Couette flow. Material parameters of Phase 5A at 30 °C, layer thickness $d = 20$ μm, flow amplitude $a = 0.17$, and flow frequency $f = 155$ Hz. Simulations of Eqs. (13) and (14) (solid line), simulations of Eq. (13) with prescribed velocity field (dotted line), and "universal" precession frequency $\alpha_2\alpha_3/(2\gamma_1^2)a^2 f$ (dot-dashed line). Experimental data from [5] (circles).

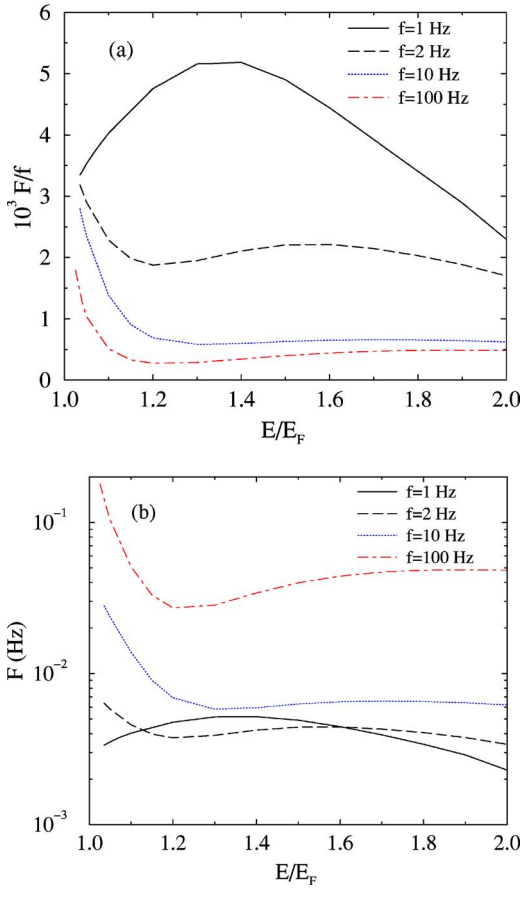

FIG. 2. (Color online) Precession frequency $F = \Omega/2\pi$ as a function of the electric field E/E_F for different frequencies of circular Couette flow. Material parameters of Phase 5A at 30 °C, layer thickness $d = 20$ μm, and flow amplitude $a = 0.2$. (a) F in units of the flow frequency f and (b) physical units.

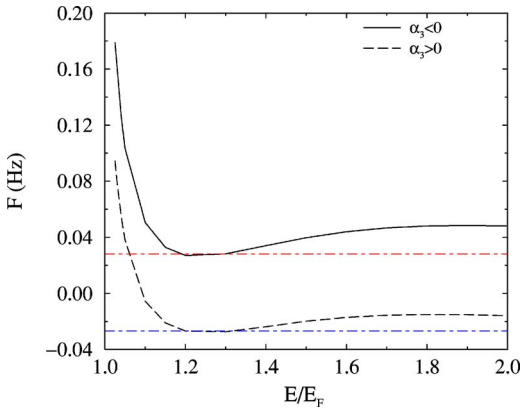

FIG. 3. (Color online) Precession frequency $F=\Omega/2\pi$ as a function of the electric field E/E_F for different sign of the viscosity coefficient α_3. Material parameters of Phase 5A at 30 °C, layer thickness $d=20$ μm, flow amplitude $a=0.2$, and flow frequency $f=100$ Hz. Simulations of Eqs. (13) and (14) (solid and dashed lines) and "universal" precession frequency $\alpha_2\alpha_3/(2\gamma_1^2)a^2f$ (dot-dashed lines).

In [5,6] an exact solution of Eqs. (13) with $\epsilon=0$ for the "prescribed" circular Couette flow $V_{,z}=ae^{it}$ was presented which leads to the "universal" precession frequency

$$\Omega_0 = 1 - \sqrt{1-\lambda a^2/(1-\lambda)^2} = \lambda/[2(1-\lambda)^2]a^2 + O(a^4), \tag{18}$$

where $\lambda=\alpha_3/\alpha_2$. For flow-aligning materials ($\lambda>0$) the precession frequency Ω_0 is positive (same sense of rotation as the elliptic shear) and negative otherwise. This result is coincided with the full numerical simulations of Eqs. (13) and (14) at an electric field well above the Hopf bifurcation: a change of the sign of the viscosity coefficient α_3 leads to the reversal of the precession (see Fig. 3).

III. VICINITY OF THE FRÉEDERICKSZ TRANSITION

Let us start with a linear and weakly nonlinear analysis of the FT, which for small-amplitude circular Couette flow is transformed into a Hopf-type bifurcation. In order to obtain analytic result we shall use a test-function approximation. For small flow amplitudes and electric fields slightly above the bend Fréedericksz transition one has $|N|\ll 1$. From the normalization of the director one can then write $n_z\approx 1-|N|^2/2$ and keep terms up to N^3 in Eqs. (13) and (14). Another simplification can be made by neglecting the term $\delta V_{,t}$ in Eq. (14) (Stokes approximation) which is expected to be valid for not too high frequencies such that $\delta\ll 1$. For typical material parameters (see the Appendix) $\gamma_1\approx 10^{-1}$ N s/m^2, $\rho\approx 10^3$ Kg/m^3, and nematic layer thickness $d=20$ μm this corresponds to $\omega\ll 250$ kHz. Also, it is convenient to go into a coordinate system rotating with the external frequency

$$N = M(z,t)e^{it}, \quad V = U(z,t)e^{it}. \tag{19}$$

Then Eqs. (13) and (14) reduce to

$$M_{,t} + iM - \epsilon\Bigg\{\pi^2e^2(1-|M|^2)M + k_1\frac{1}{2}(|M|^2)_{,zz}M + k_3\left[M_{,zz} - \frac{1}{2}M(M\bar{M}_{,zz} + \bar{M}M_{,zz})\right] + (k_3-k_2)\times\left[\frac{1}{2}MD_{,z} + M_{,z}D\right]\Bigg\} + \tilde{\alpha}_2\left(1-\frac{1}{2}|M|^2\right)U_{,z} - \frac{1}{2}(\tilde{\alpha}_2+\tilde{\alpha}_3)\times M(M\bar{U}_{,z} + \bar{M}U_{,z}) = 0, \tag{20}$$

$$\partial_z\Bigg\{\tilde{\alpha}_2\left(1-\frac{1}{2}|M|^2\right)(M_{,t}+iM) - \tilde{\alpha}_3\frac{1}{2}(|M|^2)_{,t}M + (\tilde{\eta}-\tilde{\eta}_1|M|^2)U_{,z} - \frac{1}{2}\tilde{\eta}_2M(M\bar{U}_{,z}+\bar{M}U_{,z})\Bigg\} = 0, \tag{21}$$

with $D=M\bar{M}_{,z}-\bar{M}M_{,z}$ and $\tilde{\eta}=(\tilde{\alpha}_4-\tilde{\alpha}_2+\tilde{\alpha}_5)/2$, $\tilde{\eta}_1=(-\tilde{\alpha}_2+\tilde{\alpha}_5)/2$, and $\tilde{\eta}_2=(-\tilde{\alpha}_3-\tilde{\alpha}_6)/2-\tilde{\alpha}_1$. The boundary conditions are

$$M(z=\pm 1/2)=0,$$

$$U(z=-1/2)=0, \quad U(z=+1/2)=a. \tag{22}$$

Below the instability the basic state $M=M_0(z)$, $U=U_0(z)$ corresponds to a stationary solution of Eqs. (20) and (21). For flow frequency $\omega\gg 1/\tau_d$—i.e., $\epsilon\ll 1$ (for nematic layer thickness $d=20$ μm and typical values $\gamma_1\approx 10^{-1}$ N s/m^2, $K_{33}\approx 10^{-11}$ N this corresponds to $\omega\gg 0.25$ Hz)—neglecting terms proportional to ϵ one obtains, for the basic state,

$$M_0 = X_0 + iY_0 = 0 + i\tilde{\alpha}_2a + O(a^3),$$

$$U_0 = F_0 + iH_0 = a(z+1/2) + i0 + O(a^3). \tag{23}$$

Solution (23) for M_0 discard two boundary layers at $z=\pm 1/2$ which are of thickness $\sim\sqrt{\epsilon}$, where M_0 rapidly goes to its boundary value $M_0(z=\pm 1/2)=0$.

We now perform the stability analysis of the basic state: $M=M_0+M_1(z,t)$, $U=U_0+U_1(z,t)$ with $|M_1|\ll 1$, $|U_1|\ll 1$ by using the test-function approximation (lowest-order Galerkin expansion)

$$\begin{pmatrix} M_1(z,t) \\ U_1(z,t)\end{pmatrix} = Ae^{\sigma t}\begin{pmatrix} m_1\cos(\pi z) \\ u_1\sin(2\pi z)\end{pmatrix}. \tag{24}$$

Solving the linear problem one gets for the complex growth rate

$$\sigma^2 - c_1\sigma + c_0 = 0,$$

$$c_1 = L_{11}+L_{22}, \quad c_0 = L_{11}L_{22}-L_{12}L_{21}, \tag{25}$$

where, at leading order in a [up to $O(a^2)$],

$$L_{11} = \frac{\epsilon\pi^2}{1-\beta}\left(e^2\left\{1-\frac{1-\beta\tilde{\eta}_1/\tilde{\eta}}{1-\beta}\tilde{\alpha}_2^2a^2\right\} - k_2\tilde{\alpha}_2^2a^2 - k_3\left\{1-\frac{1-\beta\tilde{\eta}_1/\tilde{\eta}}{1-\beta}\tilde{\alpha}_2^2a^2\right\}\right),$$

$$L_{12} = 1 + \frac{1-\beta(2\tilde{\eta}_1/\tilde{\alpha}_2^2 - 1)}{1-\beta}\tilde{\alpha}_2^2 a^2,$$

$$L_{21} = -1 + \frac{1+\lambda-\beta(\tilde{\eta}_2/\tilde{\alpha}_2^2 - \lambda)}{1-\beta}\tilde{\alpha}_2^2 a^2,$$

$$L_{22} = \frac{\epsilon\pi^2}{1-\beta}\left(e^2\left\{1 - \frac{3-\beta[1-2\lambda+(\tilde{\eta}_1+\tilde{\eta}_2)/\tilde{\eta}]}{1-\beta}\tilde{\alpha}_2^2 a^2\right\} - k_1\tilde{\alpha}_2^2 a^2 - k_3\left\{1 - \frac{1+\beta[1+2\lambda-(\tilde{\eta}_1+\tilde{\eta}_2)/\tilde{\eta}]}{1-\beta}\tilde{\alpha}_2^2 a^2\right\}\right). \tag{26}$$

Here $\beta = 16\tilde{\alpha}_2^2/(9\pi^2\tilde{\eta})$ and $\lambda = \tilde{\alpha}_3/\tilde{\alpha}_2$. Note that setting $\beta = 0$ the case of unperturbed (prescribed) velocity field is obtained; i.e., only Eq. (20) is considered with given $U(z,t) \equiv U_0 = a(z+1/2)$ and Eq. (21) not taken into account.

At threshold $\mathrm{Re}(\sigma) = 0$, $\mathrm{Im}(\sigma) = \omega_c$ one finds, at leading order in a,

$$e_c^2 = k_3 + \frac{1}{2}(k_1 + k_2 + 2k_3)\tilde{\alpha}_2^2 a^2,$$

$$\omega_c = 1 - \frac{1}{2}\frac{\tilde{\alpha}_2\tilde{\alpha}_3 + \beta(2\tilde{\eta}_1 - \tilde{\eta}_2 - \tilde{\alpha}_2^2 + \tilde{\alpha}_2\tilde{\alpha}_3)}{1-\beta}a^2. \tag{27}$$

Since $\omega_c \neq 0$, one has a Hopf bifurcation at $e = e_c$ which is slightly above the critical field for the usual Fréedericksz transition. The precession frequency in the laboratory coordinate system is $\Omega_c = 1 - \omega_c$. In the case of prescribed velocity field ($\beta = 0$) one gets $\Omega_{c0} = \tilde{\alpha}_2\tilde{\alpha}_3 a^2/2$, which is in agreement with Eq. (18). In the experiments and in the simulations the Hopf frequency is higher; see Figs. 1 and 2. This is in good agreement with the results of our stability analysis of the complete set of equations (20) and (21). From the numerical simulations at $f = 100$ Hz (see Fig. 2) where $\epsilon = 3.6 \times 10^{-4}$, $a = 0.2$, we found $e_c^2 = 1.06$ and $\Omega_c = 1.6 \times 10^{-3}$. Equations (27) give $e_c^2 = 1.064$ and $\Omega_c = 1.43 \times 10^{-3}$.

Our weakly nonlinear analysis for the regime slightly above the Hopf bifurcation makes use of the expansion

$$M_1 = \mu M_1^{(1)} + \mu^2 M_1^{(2)} + \mu^3 M_1^{(3)} + \cdots,$$

$$U_1 = \mu U_1^{(1)} + \mu^2 U_1^{(2)} + \mu^3 U_1^{(3)} + \cdots,$$

$$\mu = \sqrt{e^2 - e_c^2}, \quad \partial_t \to \partial_t + \mu^2\partial_T, \tag{28}$$

where the slow time $T = \mu^2 t$ has been introduced. Substituting Eqs. (28) into Eqs. (20) and (21) one obtains equations at each order in μ. The solvability condition for the equation at $O(\mu^3)$ gives the equation for the complex amplitude A defined in Eq. (24),

$$\partial_t A = [(e^2 - e_c^2)P_1 - P_3|A|^2]A, \tag{29}$$

where, at leading order in a,

$$\mathrm{Re}(P_1) = \frac{\epsilon\pi^2}{1-\beta}\left(1 - \frac{\tilde{\alpha}_2^2 a^2}{1-\beta}\{2 - \beta[1 - 2\lambda + (2\tilde{\eta}_1 + \tilde{\eta}_2)/\tilde{\eta}]/2\}\right),$$

$$\mathrm{Im}(P_1) = 0,$$

$$\mathrm{Re}(P_3) = \frac{\epsilon\pi^2}{1-\beta}\left(2k_1 + \frac{a^2}{2(1-\beta)}\left\{\tilde{\alpha}_2^2\left[-\frac{1}{2}k_1 + \frac{3}{2}k_2 + \left(3 - \frac{64}{9\pi^2}\right)k_3 - \beta\left(\frac{31}{2}k_1 + \frac{3}{2}k_2 + 9k_3\right)\right] - \tilde{\alpha}_2\tilde{\alpha}_3\left[\left(1 - \frac{64}{9\pi^2}\right)k_1 + 2\beta(5k_1 + 2k_3)\right] + \beta k_1(\tilde{\eta} + \tilde{\alpha}_2^2)(2\tilde{\eta}_1 + \tilde{\eta}_2)/\tilde{\eta}\right\}\right),$$

$$\mathrm{Im}(P_3) = \frac{a^2}{2(1-\beta)^2}\left[-\frac{64}{9\pi^2}\tilde{\alpha}_2^2(2+\lambda) + \frac{\beta}{5}(12\tilde{\eta}_1 - 6\tilde{\eta}_2 + 4\tilde{\alpha}_2^2 + 37\tilde{\alpha}_2\tilde{\alpha}_3 + 10\tilde{\alpha}_3^2)\right]. \tag{30}$$

Note that $\mathrm{Re}(P_3)$ and $\mathrm{Im}(P_3)$ can be controlled independently by choosing the flow frequency and amplitude. From Eqs. (27), (29), and (30) one gets, at leading order in a for the precession frequency (in the laboratory coordinate system) slightly above the Hopf bifurcation,

$$\Omega = \Omega_c - (e^2 - e_c^2)\Delta\Omega,$$

$$\Omega_c = \frac{1}{2}\frac{\tilde{\alpha}_2\tilde{\alpha}_3 + \beta(2\tilde{\eta}_1 - \tilde{\eta}_2 - \tilde{\alpha}_2^2 + \tilde{\alpha}_2\tilde{\alpha}_3)}{1-\beta}a^2,$$

$$\Delta\Omega \equiv \mathrm{Im}(P_1) - \frac{\mathrm{Re}(P_1)\mathrm{Im}(P_3)}{\mathrm{Re}(P_3)} = \frac{a^2}{4k_1(1-\beta)^2}\left[-\frac{64}{9\pi^2}\tilde{\alpha}_2^2(2+\lambda) + \frac{\beta}{5}(12\tilde{\eta}_1 - 6\tilde{\eta}_2 + 4\tilde{\alpha}_2^2 + 37\tilde{\alpha}_2\tilde{\alpha}_3 + 10\tilde{\alpha}_3^2)\right]. \tag{31}$$

We found from the numerical simulations, at $f = 100$ Hz, $\Delta\Omega = 0.017$, and from Eq. (31), $\Delta\Omega = 0.02$.

We may also include weak modulations of the amplitude A in the x and y directions by introducing slow space variables $X = \mu x$, $Y = \mu y$—i.e., $\partial_x \to \partial_x + \mu\partial_X$ in Eqs. (28). Then Eq. (29) is extended to a modified complex Ginzburg-Landau equation

$$\partial_t A = [(e^2 - e_c^2)P_1 - P_3|A|^2]A + C\nabla_\perp^2 A, \tag{32}$$

where $\nabla_\perp^2 = \partial_X^2 + \partial_Y^2$ and

$$C = \frac{\epsilon}{1-\beta}\frac{k_1 + k_2}{2} + O(a^2). \tag{33}$$

Equation (32) represents the well-known complex Ginzburg-Landau equation, which is the universal normal form describing a homogeneous Hopf bifurcation in an extended isotropic medium. It is well known that this equation admits dispersive waves (for a general discussion of the equation see [14]) and, in particular, rotating spirals. In fact, in the present case with real C (no linear dispersion) and large $|\mathrm{Im}(P_3)/\mathrm{Re}(P_3)|$ (large nonlinear dispersion) the relevant solutions will be spatiotemporally chaotic, as observed in the experiments [5,6]. In fact, this parameter range is singled out by the fact that there exist so-called retracting fronts, which connect the undistorted state with the distorted one and move in such a way that the (unstable) undistorted state expands [15]. For $|\mathrm{Im}(P_3)/\mathrm{Re}(P_3)|>4.8$ their velocity is larger than that of the usual "linear" fronts connecting these states and moving in the opposite direction. Then the retracting fronts dominate the dynamics which leads to spatiotemporal intermittency [15]. It would be interesting to study this effect in detail utilizing the fact that $\mathrm{Re}(P_3)$ and $\mathrm{Im}(P_3)$ can be controlled independently.

IV. WELL ABOVE THE FRÉEDERICKSZ TRANSITION

Next we consider the case of an electric field sufficiently far above E_F so that the director is distorted well away from the homeotropic orientation. We start out without flow. Then there is no preferred direction of the (mean) inclination in the plane of the layer. For small flow amplitudes $|a|\ll 1$ one can treat the problem in a perturbative way by introducing a slow time $T=a^2t$ that modulates the periodic behavior on the fast time scale t. Then $N=N(z,t,T)$ and $V=V(z,t,T)$, $\partial_t\to\partial_t+a^2\partial_T$, and one can formulate a systematic perturbation expansion of the form

$$N=N_0+aN_1+a^2N_2+\cdots,$$

$$G=aG_1+a^2G_2+\cdots, \tag{34}$$

where we introduced the complex velocity gradient $G=V_{,z}$. Clearly there is no zeroth-order contribution to G [see Eqs. (16) and (17)]. Substituting Eqs. (34) into Eqs. (13) and (14) one obtains, at zeroth order in a,

$$N_{0,t}-\epsilon\Big\{\pi^2e^2(1-|N_0|^2)N_0-k_1n_{z0}n_{z0,zz}N_0+k_3\Big[N_{0,zz}-\frac{1}{2}N_0(N_0\overline{N_{0,zz}}+\overline{N_0}N_{0,zz})\Big]-(k_3-k_2)\times\Big[\frac{1}{2}N_0(B_0^2+iB_{0,z})+iN_{0,z}B_0\Big]\Big\}=0, \tag{35}$$

where $n_{z0}=\sqrt{1-|N_0|^2}$ and $B_0=i(N_0\overline{N}_{0,z}-\overline{N_0}N_{0,z})$. Equation (35) has a t-independent solution of the form

$$N_0=R_0(z)e^{i\Phi_0(T)}, \tag{36}$$

where $\Phi_0(T)$ describes the slow rotation of the projection of the director averaged over the flow period which is undetermined at this order. Then one has $B_0=0$ and, for R_0,

$$\pi^2e^2(1-R_0^2)R_0-k_1n_{z0}n_{z0,zz}R_0+k_3(1-R_0^2)R_{0,zz}=0, \tag{37}$$

which is the equation for the standard bend Fréedericksz transition giving the threshold $e_c=1$ for the existence of the nontrivial solution with $R_0(z=\pm1/2)=0$.

At first order in a one has a system of linear equations for N_1 and G_1,

$$N_{1,t}-\epsilon\hat{\mathcal{L}}_N(N_0|N_1)+\hat{\mathcal{L}}_G(N_0|G_1)=0, \tag{38}$$

$$-\hat{\mathcal{M}}_N(N_0|N_1)+\delta G_{1,t}-\hat{\mathcal{M}}_G(N_0|G_1)=0, \tag{39}$$

where the linear operators

$$\begin{aligned}\hat{\mathcal{L}}_N(N_0|N_1)=&\pi^2e^2(1-|N_0|^2)N_1-\pi^2e^2N_0(N_0\overline{N_1}+\overline{N_0}N_1)\\&-k_1n_{z0}n_{z0,zz}N_1-k_1N_0(n_{z0}n_{z1,zz}+n_{z1}n_{z0,zz})\\&+k_3\Big[N_{1,zz}-\frac{1}{2}N_1(N_0\overline{N_{0,zz}}+\overline{N_0}N_{0,zz})\Big]\\&-k_3\frac{1}{2}N_0(N_0\overline{N_{1,zz}}+\overline{N_0}N_{1,zz}+N_{0,zz}\overline{N_1}+\overline{N_{0,zz}}N_1)\\&-(k_3-k_2)i\Big(\frac{1}{2}N_0B_{1,z}+N_{0,z}B_1\Big),\end{aligned} \tag{40}$$

$$\hat{\mathcal{L}}_G(N_0|G_1)=\tilde{\alpha}_2n_{z0}G_1-\frac{1}{2}(\tilde{\alpha}_2+\tilde{\alpha}_3)n_{z0}N_0(N_0\overline{G_1}+\overline{N_0}G_1), \tag{41}$$

$$\hat{\mathcal{M}}_N(N_0|N_1)=\partial_{zz}^2\{\tilde{\alpha}_2n_{z0}N_{1,t}+\tilde{\alpha}_3N_0n_{z1,t}\}, \tag{42}$$

$$\begin{aligned}\hat{\mathcal{M}}_G(N_0|G_1)=\partial_{zz}^2\Big\{&\Big[\frac{1}{2}(-\tilde{\alpha}_2+\tilde{\alpha}_4+\tilde{\alpha}_5)-\frac{1}{2}(-\tilde{\alpha}_2+\tilde{\alpha}_5)|N_0|^2\Big]G_1\\&+\frac{1}{2}\Big[\frac{1}{2}(\tilde{\alpha}_3+\tilde{\alpha}_6)+\tilde{\alpha}_1(1-|N_0|^2)\Big]N_0\\&\times(N_0\overline{G_1}+\overline{N_0}G_1)\Big\},\end{aligned} \tag{43}$$

and

$$n_{z1}=-\frac{1}{2n_{z0}}(N_0\overline{N_1}+\overline{N_0}N_1),$$

$$B_1=i(N_0\overline{N_{1,z}}-\overline{N_0}N_{1,z}-N_{0,z}\overline{N_1}+\overline{N_{0,z}}N_1). \tag{44}$$

Since one has time periodic boundary conditions for the velocity in case of Couette flow (16) or a time-periodic pressure gradient for Poiseuille flow (17), the solution of the homogeneous linear system (38) and (39) will have the form

$$N_1=e^{it}N_{1+}+e^{-it}N_{1-}, \tag{45}$$

$$G_1 = e^{it}G_{1+} + e^{-it}G_{1-}, \tag{46}$$

with time averages $\langle N_1\rangle_t=0$ and $\langle G_1\rangle_t=0$ where $\langle F\rangle_t = (2\pi)^{-1}\int_t^{t+2\pi} F dt$. Note that for the prescribed circular Couette flow $G_{1+}=1$ and $G_{1-}=0$. Elliptical flow is obtained by superposing left- and right-rotating contributions.

For flow frequency $\omega \gg 1/\tau_d$ (i.e., $\epsilon \ll 1$) one can treat Eq. (38) as a boundary layer problem. The boundary layers at $z = \pm 1/2$ are of thickness $\sim\sqrt{\epsilon}$. Then, solving Eq. (38) in the bulk where one can neglect the terms proportional to ϵ and near to the boundaries one obtains at leading order in ϵ after the matching

$$\begin{aligned}
N_1 = &- i\tilde{\alpha}_2 n_{z0}(-e^{it}G_{1+} + e^{-it}G_{1-}) \\
&+ i\frac{1}{2}(\tilde{\alpha}_2 + \tilde{\alpha}_3) n_{z0} N_0 [-e^{it}(N_0\overline{G_{1-}} + \overline{N_0}G_{1+}) \\
&+ e^{-it}(N_0\overline{G_{1+}} + \overline{N_0}G_{1-})] \\
&- i\tilde{\alpha}_2 \left[\exp\left(-\frac{i+1}{\sqrt{2}} \frac{1/2+z}{\sqrt{\epsilon k_3}} \right) G_{1+}(-1/2) \right. \\
&\left. + \exp\left(-\frac{i+1}{\sqrt{2}} \frac{1/2-z}{\sqrt{\epsilon k_3}} \right) G_{1+}(1/2) \right] e^{it} \\
&+ i\tilde{\alpha}_2 \left[\exp\left(-\frac{-i+1}{\sqrt{2}} \frac{1/2+z}{\sqrt{\epsilon k_3}} \right) G_{1-}(-1/2) \right. \\
&\left. + \exp\left(-\frac{-i+1}{\sqrt{2}} \frac{1/2-z}{\sqrt{\epsilon k_3}} \right) G_{1-}(1/2) \right] e^{-it}.
\end{aligned} \tag{47}$$

At second order in a one has the system of inhomogeneous linear equations for N_2 and G_2:

$$N_{2,t} - \epsilon\hat{\mathcal{L}}_N(N_0|N_2) + \hat{\mathcal{L}}_G(N_0|G_2) = \mathrm{rhs}_N, \tag{48}$$

$$-\hat{\mathcal{M}}_N(N_0|N_2) + \delta G_{2,t} - \hat{\mathcal{M}}_G(N_0|G_2) = \mathrm{rhs}_G, \tag{49}$$

with inhomogeneities

$$\begin{aligned}
\mathrm{rhs}_N = &- N_{0,T} + \epsilon \left\{ -\pi^2 e^2 N_0 |N_1|^2 - \pi^2 e^2 N_1 (N_0\overline{N_1} + \overline{N_0}N_1) \right. \\
&- k_1 N_0 n_{z1} n_{z1,zz} - k_1 N_1 (n_{z0} n_{z1,zz} + n_{z1} n_{z0,zz}) \\
&- k_3 \frac{1}{2} N_0 (N_1 \overline{N_{1,zz}} + \overline{N_1} N_{1,zz}) - k_3 \frac{1}{2} N_1 (N_0 \overline{N_{1,zz}} + \overline{N_0} N_{1,zz} \\
&+ N_{0,zz}\overline{N_1} + \overline{N_{0,zz}} N_1) - (k_3 - k_2) i \left(\frac{1}{2} N_1 B_{1,z} + N_{1,z} B_1 \right. \\
&\left. \left. + \frac{1}{2} N_0 B_1^2 \right) \right\} - \tilde{\alpha}_2 n_{z1} G_1 + \frac{1}{2}(\tilde{\alpha}_2 + \tilde{\alpha}_3) n_{z0} N_0 \\
&\times (N_1\overline{G_1} + \overline{N_1}G_1) + \frac{1}{2}(\tilde{\alpha}_2 + \tilde{\alpha}_3)(n_{z0}N_1 + n_{z1}N_0) \\
&\times (N_0\overline{G_1} + \overline{N_0}G_1),
\end{aligned} \tag{50}$$

$$\begin{aligned}
\mathrm{rhs}_G = &\partial_{zz}^2 \left\{ \tilde{\alpha}_2 n_{z0} N_{0,T} + \tilde{\alpha}_2 n_{z1} N_{1,t} + \tilde{\alpha}_3 N_1 n_{z1,t} - \frac{1}{2}(-\tilde{\alpha}_2 + \tilde{\alpha}_5) \right. \\
&\times (N_0\overline{N_1} + \overline{N_0}N_1) G_1 + \frac{1}{2} \left[\frac{1}{2}(\tilde{\alpha}_3 + \tilde{\alpha}_6) \right. \\
&\left. + \tilde{\alpha}_1 (1 - |N_0|^2) \right] N_0 \times (N_1\overline{G_1} + \overline{N_1}G_1) \\
&+ \frac{1}{2} \left[\left(\frac{1}{2}(\tilde{\alpha}_3 + \tilde{\alpha}_6) + \tilde{\alpha}_1 (1 - |N_0|^2) \right) N_1 \right. \\
&\left. \left. - \tilde{\alpha}_1 (N_0\overline{N_1} + \overline{N_0}N_1) N_0 \right] (N_0\overline{G_1} + \overline{N_0}G_1) \right\}.
\end{aligned} \tag{51}$$

We are looking for a 2π-periodic solution of the system (48) and (49). One can write

$$N_2 = N_{2st} + N_{2os}, \quad G_2 = G_{2st} + G_{2os}, \tag{52}$$

where $\langle N_{2os}\rangle_t=0$, $\langle G_{2os}\rangle_t=0$ and $N_{2st}=r_2 e^{i\Phi_0}$, $G_{2st}=g_2 e^{i\Phi_0}$ with r_2 and g_2 time independent. The homogeneous system (38) and (39) has the time-independent Null eigenvector $(iN_0;0)$ and the solvability condition for the inhomogeneous system (48) and (49) will take the form

$$\langle\langle -i\overline{N_0}[\epsilon\hat{\mathcal{L}}_N(N_0|N_{2st}) - \hat{\mathcal{L}}_G(N_0|G_{2st}) + \mathrm{rhs}_N]\rangle\rangle = 0, \tag{53}$$

where $(-i\overline{N_0};0)$ is the null eigenvector of the problem adjoint to Eqs. (38) and (39) and we define the scalar product

$$\langle\langle UF\rangle\rangle = \int_{-1/2}^{1/2} dz \frac{1}{2\pi} \int_t^{t+2\pi} UF dt. \tag{54}$$

The real part of the solvability condition (53) gives the equation for Φ_0 whereas the imaginary part gives the equation for N_{2st}, G_{2st}.

Taking the solution (47) one obtains from Eq. (53) at leading order in ϵ the evolution equation for Φ_0 of the form

$$\Phi_{0,T} = -f_1 + f_2 \sin(2\Phi_0), \tag{55}$$

where

$$\begin{aligned}
f_1 = &\frac{1}{2}\tilde{\alpha}_2\tilde{\alpha}_3 \langle R_0^2 (|G_{1-}|^2 - |G_{1+}|^2)\rangle_z / \langle R_0^2\rangle_z + (2k_3\epsilon)^{3/2} \\
&\times \frac{1}{2} \left[-\tilde{\alpha}_2\tilde{\alpha}_3 + \frac{2k_1 - 2k_2 + k_3}{k_3} \tilde{\alpha}_2^2 \right] I_1
\end{aligned}$$

$$f_2 = (2k_3\epsilon)^{3/2} \frac{1}{2} \frac{k_1 + 2k_3 - 2k_2}{k_3} \tilde{\alpha}_2^2 I_2, \tag{56}$$

with $\langle F\rangle_z = \int_{-1/2}^{1/2} F dz$ and

$$\begin{aligned}
I_1 = &\{[R_{0,z}(-1/2)]^2 [|G_{1-}(-1/2)|^2 - |G_{1+}(-1/2)|^2] \\
&+ [R_{0,z}(1/2)]^2 [|G_{1-}(1/2)|^2 - |G_{1+}(1/2)|^2]\} / \langle R_0^2\rangle_z,
\end{aligned}$$

$$\begin{aligned}
I_2 = &\{[R_{0,z}(-1/2)]^2 [G_{1-}(-1/2) G_{1+}(-1/2) + \overline{G_{1-}}(-1/2) \\
&\times \overline{G_{1+}}(-1/2)] + [R_{0,z}(1/2)]^2 [G_{1-}(1/2) G_{1+}(1/2) \\
&+ \overline{G_{1-}}(1/2) \overline{G_{1+}}(1/2)]\} / \langle R_0^2\rangle_z.
\end{aligned} \tag{57}$$

For $f_1 > f_2$, Eq. (55) describes slow precession of the director. Neglecting the elasticity ($\epsilon=0$) one has, for the precession frequency,

$$\Omega \sim \frac{\alpha_2\alpha_3}{\gamma_1^2}a^2\omega, \tag{58}$$

which coincides with Eq. (18).

Slow x and y variations can be included in the form $X = ax$, $Y=ay$, $\partial_x \to a\partial_X$, $\partial_y \to a\partial_Y$, and $\Phi_0=\Phi_0(T,X,Y)$. This leads on the right-hand side of Eq. (55) to the additional terms

$$C_1(\partial_{XX}+\partial_{YY})\Phi_0 + C_2\{\sin(2\Phi_0)[(\partial_X\Phi_0)^2 - (\partial_Y\Phi_0)^2 - 2\partial_{XY}\Phi_0] - \cos(2\Phi_0)[\partial_{XX}\Phi_0 - \partial_{YY}\Phi_0 + 2(\partial_X\Phi_0)(\partial_Y\Phi_0)]\}, \tag{59}$$

where

$$C_1 = \frac{\epsilon}{2}[k_1 + k_2 + (k_3-k_2)\langle R_0^4\rangle_z/\langle R_0^2\rangle_z],$$

$$C_2 = \frac{\epsilon}{2}[k_1 - k_2 - (k_3-k_2)\langle R_0^4\rangle_z/\langle R_0^2\rangle_z]. \tag{60}$$

For $f_1 > f_2$, Eq. (55) with (59) describes diffusive phase waves that propagate on the background of the slow director precession. Typical examples of the inhomogeneous director distribution in the plane of nematic layer are umbilics (point defects with topological index ± 1) formed in homeotropically oriented nematic liquid crystals with negative dielectric anisotropy in an electric field above the Fréedericksz transition [1]. Considering the case of circular flow ($f_2=0$) and the one-elastic-constant approximation ($k_1=k_2=k_3$) one can find the simple solution

$$\Phi_0 = -f_1 t + \tan^{-1}\left(\frac{Y-Y_1}{X-X_1}\right) - \tan^{-1}\left(\frac{Y-Y_2}{X-X_2}\right), \tag{61}$$

which corresponds to a pair of rotating umbilics located at (X_1,Y_1) and (X_2,Y_2) with opposite topological index as observed in experiments under low-frequency elliptical Couette flow [16]. Another type of solution of Eqs. (55) with (59) is given by

$$\Phi_0 = f_1 t + \frac{f_1}{2C_1}[(X-X_0)^2 + (Y-Y_0)^2] \tag{62}$$

and represents outgoing circular waves with the square of the radius proportional to the local wave number. Such target-pattern wave sources have been observed under high-frequency flow excited by a piezocrystal [8].

For $f_1 < f_2$ the system becomes excitable. Whereas homogeneous precession is then excluded, wave trains with wavelength below a threshold should still be possible.

V. DISCUSSION

In Fig. 1 we present results for the dependence of the precession frequency $F=\Omega/2\pi$ on the reduced applied electric field E/E_F for the case of circular Couette flow with $a=0.17$, $\epsilon=2.5\times10^{-4}$, and $\delta=1.5\times10^{-3}$ for the material parameters of Phase 5A at 30 °C (see the Appendix), corresponding to the experiments with $A_x=A_y=3.4$ μm, $d=20$ μm, and flow frequency $f=155$ Hz [5]. The full simulations (solid line) compare well with the experiments (circles). The remaining discrepancies may result from inaccuracies of the experiments and uncertainties in the parameters. For comparison we have included the results obtained from Eq. (13) with the prescribed velocity profile (dotted line). Whereas the high-field limit comes out fairly accurately, the structures at lower fields, in particular near the Hopf bifurcation, are not reproduced. Also included in Fig. 1 is the frequency $\Omega_0/2\pi$, Eq. (18), obtained by imposing the prescribed velocity profile and neglecting elasticities (dot-dashed line). Our analytical calculations clearly demonstrate that the back flow effect is responsible for the high precession frequency Ω at the Hopf bifurcation and the sharp decrease of Ω slightly above the onset. The results of weakly nonlinear analysis are in a good quantitative agreement with numerical simulations.

In Fig. 2 we present results from simulations as before, but for various flow frequencies f. Whereas in Fig. 2(a) the reduced precession frequency—i.e., F/f—is shown, we give in Fig. 2(b) the frequency in physical units. One can see that depending on f the precession frequency can either increase or decrease above the onset of the Hopf bifurcation. The increase results from the dominance of the effect of the elasticities, which is strongest at low frequency.

Figure 3 demonstrates the influence of the sign of the viscosity coefficient α_3 on the precession frequency. The solid line is obtained for the material parameters of Phase 5A at 30 °C with $\alpha_3=-1.5\times10^{-3}$ N s/m^2 whereas for the dashed line $\alpha_3=+1.5\times10^{-3}$ N s/m^2 was taken. At the Hopf bifurcation the precession frequency Ω is positive and change sign for $\alpha_3>0$ at high electric fields (i.e., the direction of the precession is opposite to the elliptic shear). For either sign of α_3 the precession frequency approaches the "universal" value given by Eq. (18) at high electric fields,

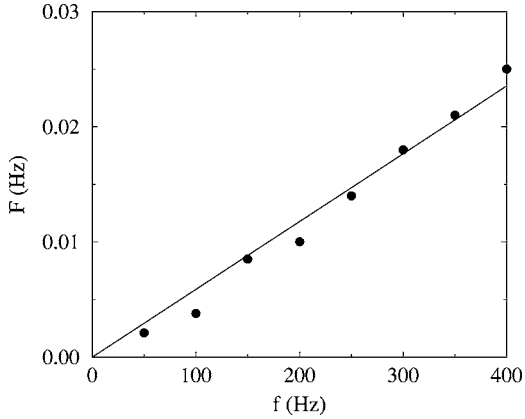

FIG. 4. Precession frequency $F=\Omega/2\pi$ as a function of the flow frequency $f=\omega/2\pi$ for circular Poiseuille flow. Material parameters of MBBA at 25 °C, layer thickness $d=20$ μm, flow amplitude $a=0.15$, and $E/E_F=2.6$. Simulations of Eqs. (13) and (14) (solid line). Experimental data from [17] (circles).

where the average director orientation is nearly in the plane of the nematic layer (except at the boundaries) and where the back flow effects become less important.

Recently some experiments on circular Poiseuille flow have been performed [17]. In Fig. 4 the precession frequency as a function of the flow frequency at a rather high electric field is compared with the simulations. In this range one expects to good accuracy a linear relation, as shown by the simulation. The slope agrees within 2% with that given by the universal limit, Eq. (18). With increasing flow frequency the universal limit should be valid to progressively lower fields.

It would be interesting to study experimentally in detail the different regimes where nonlinear waves occur. For this purpose Poiseuille flow is probably preferable because it can be applied in a more controlled way. From the theoretical side it should be possible to introduce a more general phase description that is valid far away from umbilics in the whole range of the electric field.

ACKNOWLEDGMENTS

We wish to thank W. Pesch for helpful discussions and critical reading of the manuscript. Financial support by DFG (Grants Kr690/14-1 and Kr690/22-1) and RFBR (Grant Nos. 05-02-16548 and 05-02-97907) is gratefully acknowledged.

APPENDIX

Phase 5A material parameters used (at 30 °C): viscosities ($\times 10^{-3}$ N s/m^2) $\alpha_1=-39.0$, $\alpha_2=-109.3$, $\alpha_3=-1.5$, $\alpha_4=56.3$, $\alpha_5=82.9$, and $\alpha_6=-24.9$ and elastic moduli ($\times 10^{-12}$ N) $K_{11}=9.8$, $K_{22}=4.6$, and $K_{33}=12.7$.

MBBA material parameters used (at 25 °C): viscosities ($\times 10^{-3}$ N s/m^2) $\alpha_1=-18.1$, $\alpha_2=-110.4$, $\alpha_3=-1.1$, $\alpha_4=82.6$, $\alpha_5=77.9$, and $\alpha_6=-33.6$ and elastic moduli ($\times 10^{-12}$ N) $K_{11}=6.66$, $K_{22}=4.2$, and $K_{33}=8.61$.

[1] A. Rapini, J. Phys. (Paris) **34**, 629 (1973); A. Rapini, L. Léger, and A. Martinet, J. Phys. (Paris), Colloq. **36**, C1-189 (1975).

[2] E. Santamato, B. Daino, M. Romagnoli, M. Settembre, and Y. R. Shen, Phys. Rev. Lett. **57**, 2423 (1986).

[3] L. Marrucci, G. Abbate, S. Ferraiuolo, P. Maddalena, and E. Santamato, Phys. Rev. A **46**, 4859 (1992).

[4] E. Brasselet, B. Doyon, T. V. Galstian, and L. J. Dube, Phys. Rev. E **67**, 031706 (2003).

[5] T. Börzsönyi, Á. Buka, A. P. Krekhov, O. A. Scaldin, and L. Kramer, Phys. Rev. Lett. **84**, 1934 (2000).

[6] A. P. Krekhov, T. Börzsönyi, P. Tóth, Á. Buka, and L. Kramer, Phys. Rep. **337**, 171 (2000).

[7] A. N. Chuvyrov, Zh. Eksp. Teor. Fiz. **82**, 761 (1982) [Sov. Phys. JETP **55**, 451 (1982)].

[8] A. N. Chuvyrov, O. A. Scaldin, and V. A. Delev, Mol. Cryst. Liq. Cryst. Sci. Technol., Sect. A **215**, 187 (1992).

[9] F. Scudieri, Ann. Phys. (Paris) **3**, 311 (1978).

[10] P. Pieranski and E. Guyon, Phys. Rev. Lett. **39**, 1280 (1977).

[11] E. Dubois-Violette and F. Rothen, J. Phys. (Paris) **39**, 1039 (1978).

[12] E. Dubois-Violette and P. Manneville, in *Pattern Formation in Liquid Crystals*, edited by A. Buka and L. Kramer (Springer-Verlag, New York, 1996).

[13] P. G. de Gennes and J. Prost, *The Physics of Liquid Crystals* (Clarendon Press, Oxford, 1993).

[14] I. S. Aranson and L. Kramer, Rev. Mod. Phys. **74**, 99 (2002).

[15] P. Coullet and L. Kramer, Chaos **14**, 244 (2004).

[16] J.-M. Dreyfus and P. Pieranski, J. Phys. (Paris) **42**, 459 (1981).

[17] P. Tóth, Ph.D. thesis, Universität Bayreuth, Bayreuth, 2001 (in German).